Origin and properties of the wetting layer and early evolution of epitaxially strained thin films

Helen R. Eisenberg* and Daniel Kandel†
Department of Physics of Complex Systems, Weizmann Institute of Science, Rehovot 76100, Israel
(Received 15 January 2002; published 30 October 2002)

We showed that a wetting layer in epitaxially strained thin films, which decreases with increasing lattice mismatch strain, arises due to the variation of nonlinear elastic free energy with film thickness. We calculated how and at what thickness a flat film becomes unstable to perturbations of varying size for films with both isotropic and anisotropic surface tension. We showed that anisotropic surface tension gives rise to a metastable enlarged wetting layer. The perturbation amplitude needed to destabilize this wetting layer decreases with increasing lattice mismatch. We also studied the early evolution of epitaxially strained films. We found that film growth is dependent on the mode of material deposition. The growth of a perturbation in a flat film is found to obey robust scaling relations. These scaling relations differ for isotropic and anisotropic surface tension.

DOI: 10.1103/PhysRevB.66.155429 PACS number(s): 68.55.Jk, 81.15.Aa

I. INTRODUCTION

The growth of epitaxially strained thin films, in which there is lattice mismatch between the substrate and the film, is of major importance in the fabrication of semiconductor and optoelectronic devices. The lattice mismatch generates strain in the deposited film, which can cause film instability unfavorable to uniform flat film growth. The strained film can relax either by the introduction of dislocations or by the formation of coherent (dislocation-free) islands on the film surface via surface diffusion. These coherent islands can self-organize to create periodic arrays which can be utilized to create quantum dot structures of electronic significance. Understanding and predicting strained thin-film evolution is important for the improved fabrication of semiconductor devices.

Early film growth tends to occur via coherent island formation as there is an energy barrier to the introduction of dislocations. Dislocations occur at island edges once islands reach a certain size, since the large stress at island edges provides a pathway for dislocation formation.[1] We only consider dislocation-free films, since many experiments show an absence of dislocations (see, e.g., Refs. 1 and 2) especially in early film evolution.

The current work sheds light on the following two problems: First, it has been observed experimentally that dislocation-free flat films of less than a certain thickness (the critical wetting layer) are stable to surface perturbations, while thicker films are unstable.[2–10] The thickness of the wetting layer is substance dependent and decreases with increasing lattice mismatch strain,[6–10] $\varepsilon=(a_s-a_f)/a_f$, where a_s and a_f are the substrate and film lattice constants. Above the critical wetting layer, three-dimensional 3D coherent islands form. Despite considerable effort, the physics of the critical wetting layer is poorly understood. Namely, why is there a critical, stable wetting layer and what controls its thickness? As in most cases heteroepitaxial growth is done below the roughening transition, how does anisotropic surface tension affect the thickness of the critical wetting layer? The second question we address is how does continuous material deposition affect the early evolution of thin films?

Previous work about the existence and nature of the critical wetting layer can be split into two categories: those which looked at the dynamic stability of a flat film to small perturbations,[11,12] and those which looked at whether a flat film is energetically favorable to a film with fully formed faceted islands.[13–16]

The research in the first category addressed substances with isotropic surface tension. In these works physical parameters (lattice mismatch or surface tension) which differ between the substrate and film were smoothly varied over the substrate-film interface in order to avoid nonanalyticities. The effect of such smoothing was to create a wetting layer. While the choice of a smoothing length of the order of a lattice parameter is physically reasonable, none of these works gave a physical explanation for the smoothing of material parameters over the interface or tried to physically calculate the smoothing length or form of the transition.

The research in the second category typically used physically motivated methods in order to determine the free energy of a flat film of varying thickness. Tersoff[13] and Roland and Gilmer[16] both used empirical potential methods to determine the chemical energy of flat films of Ge/Si(001). Tersoff[13] then compared this chemical potential with that of bulk strained Ge in order to determine whether it is preferable to form islands and to predict a wetting layer of 3 ML. Roland and Gilmer[16] saw some evidence of clustering in thicker films in molecular-dynamics simulations. Daruka and Barabási[14] used an expression for the free energy of a flat film of varying depths, which fits the results of the earlier works,[13,16] in order to compare the energies of flat films and films with fully faceted islands, whose energies were calculated using continuum elasticity. They saw a wetting layer, which increased with decreasing lattice mismatch. Wang *et al.*[15] used *ab initio* methods in order to determine the formation energy of flat films of varying depths of InAs/GaAs(100). They compared this energy with that of a thinner film with fully faceted islands whose energies were calculated using continuum elasticity. All the above works did not study the issue of when a flat film becomes unstable to small monolayer perturbations or the dynamics of growth.

In this paper we show that the variation of nonlinear elastic free energy with film thickness can give rise to a wetting layer, which decreases with increasing lattice mismatch

 ©2002 The American Physical Society

strain. We show how and at what depth a flat film becomes unstable to perturbations of varying size for films with both isotropic and anisotropic surface tension. This provides a more realistic estimate of critical wetting-layer thickness than the studies described above, for films in which islands grow from small surface perturbations rather than being immediately nucleated on the flat film. This mode of growth has been seen in many experimental systems,[7–9,17] especially for films with small lattice mismatch, $\varepsilon < 2.5\%$. As discussed below, we study the evolution of these small perturbations and observe island faceting. We show that anisotropic surface tension gives rise to a metastable enlarged wetting layer. The perturbation amplitude needed to destabilize this wetting layer decreases with increasing lattice mismatch.

The effects of material deposition on early thin-film evolution was addressed by Chiu and Gao,[11] who looked at the evolution of strained films with isotropic surface tension when material deposition is constant in the direction perpendicular to the film surface, corresponding to liquid phase epitaxy. In the present paper we look at thin-film growth when material deposition is constant in the direction perpendicular to the film surface, and when deposition is at a steady rate in the y direction (vertical to the interface between the film and the substrate), corresponding to any directed deposition (e.g, molecular-beam epitaxy). The latter is a much more common method of material deposition in strained film growth. We found that the type of evolution seen depends on the direction of material deposition. When the deposition is constant in the vertical y direction, the film evolves according to the linear evolution equation, even after the surface is no longer a sine function and cusp formation occurs. When deposition is constant and perpendicular to the surface, cusp formation is slowed down at very high deposition rates and the surface shows signs of reaching a steady-state morphology. We also studied thin-film evolution for faceting films, and found robust scaling laws for film growth.

The paper is organized as follows. In Sec. II we formulate the problem. In Sec. III we present the general results of linear stability analysis. In Sec. IV we describe how we calculated the variation of the nonlinear elastic free energy of a flat film with film thickness. It is this variation which gives rise to the wetting layer. Calculations were carried out using a ball-and-spring model in order to determine general qualitative behavior. Section V describes the results of the numerical simulations of thin-film evolution without material deposition, and in particular the metastability of the wetting layer. Section VI describes the results of the numerical simulations of thin-film growth with material deposition. Some of the results on thin-film growth without deposition and a brief description of the ball-and-spring model for calculating the free energy of a flat film appear in our earlier paper.[18]

II. PROBLEM FORMULATION

We model the evolution of a thin film on a substrate using continuum theory. The lattice mismatch between the film and the substrate creates a strain in the film, ε. Both the substrate and the film are assumed to be elastically isotropic with the same elastic constants. The surface of the solid is at $y = h(x,t)$ and the film is in the $y>0$ region with the film-substrate interface at $y=0$. The system is modeled to be invariant in the z direction, and all quantities are calculated for a section of unit width in that direction. This is consistent with plane strain where the solid extends infinitely in the z direction and hence all strains in this direction vanish, i.e., $e_{xz}=e_{yz}=e_{zz}=0$. We assume there is no material mixing between the substrate and the film.

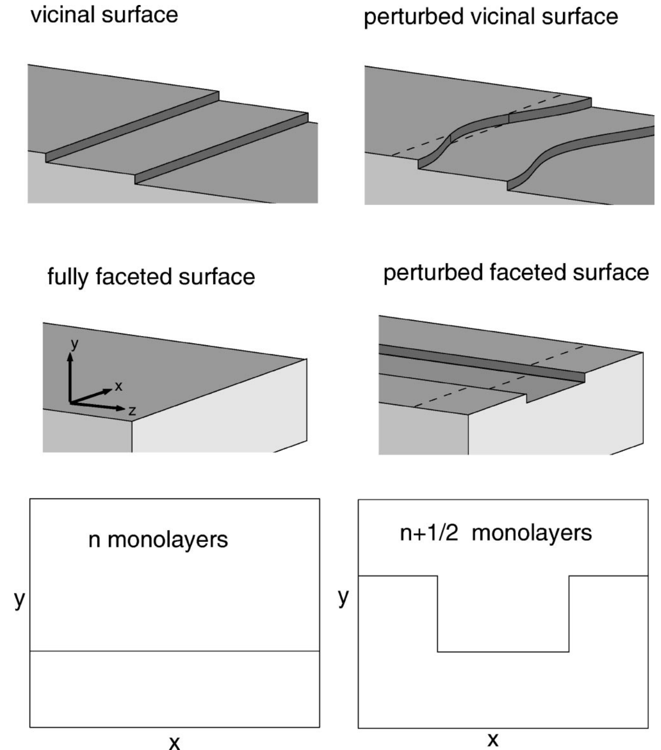

FIG. 1. Perturbations of vicinal and fully faceted surfaces. The dotted lines represent the cross sections taken in the x-y plane which are shown in the bottom graphs. The figure shows that nucleation of new steps is needed in order to perturb a facet, but not in order to perturb a surface vicinal in the z direction.

All the results mentioned in this paper relate to vicinal surfaces with a very small miscut angle in the z direction (see Fig. 1). Experimentally, surfaces often have such a small miscut, as it is very difficult to grow a perfect facet. In such surfaces there is no finite-energy barrier for the formation of an infinitesimal perturbation on the surface, since such a perturbation involves only step motion and bending, and no nucleation of new steps. For a faceted surface with no miscut in the z direction there is a finite-energy barrier for the formation of an infinitesimal perturbation associated with nucleation of step pairs.

The continuum approximation in the lateral direction (the x-z plane) is valid, as the film is infinite in the z direction and the smallest lateral surface features we study have widths of tens of atoms. However, in the vertical y direction the films we study are sometimes only a few monolayers thick. Is the continuum model valid for such a film? Can inherently discrete system properties, such as the change in free energy as a monolayer is added, be interpolated to films of a noninteger number of monolayers?

First, consider fully faceted films. As can be seen in Fig. 1, there is a qualitative difference between films with integer and noninteger numbers of monolayers, and so discrete system properties cannot be interpolated to films with a noninteger number of monolayers. Hence for such films continuum models are not expected to give accurate results. To accurately model fully faceted film growth, the discrete nature of the steps needs to be taken into account using atomistic models and simulations. Modeling large systems in such a manner is currently beyond computational capabilities. However, as can be seen in Fig. 1, the above arguments do not apply to vicinal surfaces. In this case a perturbation changes the morphology in a smooth manner without any nucleation of steps. Therefore it is possible to estimate the properties of films with a noninteger number of monolayers by interpolating the results of films of integer numbers of monolayers. Thus, a continuum model should adequately describe thin-film growth behavior for slightly vicinal surfaces.

We assume that surface diffusion is the dominant mass transport mechanism. Gradients in the chemical potential produce a drift of surface atoms with an average velocity, v, given by the Nernst-Einstein relation

$$v=-\frac{D_s}{k_BT}\frac{\partial\mu}{\partial s}, \tag{1}$$

where D_s is the surface diffusion coefficient, s is the arc length, T is the temperature, k_B is the Boltzmann constant, and μ is the chemical potential at the surface, i.e., it is the increase in free energy when an atom is added to the solid surface at the point of interest. Taking the divergence of the surface current produced by the atom drift gives an expression for the surface movement,[19]

$$\frac{\partial h}{\partial t}=\frac{D_s\eta\Omega}{k_BT}\frac{\partial}{\partial x}\frac{\partial\mu}{\partial s}, \tag{2}$$

where η is the number of atoms per unit area on the solid surface and Ω is the atomic volume.

In the continuum approximation $\mu=\Omega\,\delta F/\delta h$, where F is the free energy of the solid and $\delta F/\delta h$ is the functional derivative of F. The free energy is composed of elastic and surface terms:

$$F=F_{el}+\int dx\;\gamma\sqrt{1+(\partial h/\partial x)^2}, \tag{3}$$

where γ is the surface tension and F_{el} is the elastic free energy including any elastic contributions to the surface tension.

In general the elastic free energy can be written as $F_{el}=F_{el}^{(0)}+\delta F_{el}$, where $F_{el}^{(0)}$ is the elastic free energy of a zero-strain reference state. The elastic free energy can be written in terms of the elastic free-energy density, f_v, as $F_{el}=\int dx dy f_v$. f_v is expanded as a power series in the strain: $f_v=f_v^{(0)}+\sigma_{ij}^{(0)}e_{ij}+\frac{1}{2}c_{ijkl}e_{ij}e_{kl}+\cdots$, where $f_v^{(0)}$ is the free-energy density in the zero-strain reference state, $\sigma_{ij}^{(0)}$ is the stress in the reference state, and c_{ijkl} are the elastic coefficients of the material. In linear elasticity theory, deformations are assumed to be small and so terms of third order and higher are neglected. The stress-strain relationship is given by $\sigma_{ij}=\partial f_v/\partial e_{ij}$, which under linear elasticity gives Hooke's law:

$$\sigma_{ij}=\sigma_{ij}^{(0)}+c_{ijkl}e_{kl}. \tag{4}$$

We now briefly describe the equations which need to be satisfied in order to completely determine the equilibrium stress and strain in an elastic body. An elastic solid must satisfy the equations of mechanical equilibrium at every point in its interior (see, e.g., Ref. 20):

$$\partial_j\sigma_{ij}+\xi_i=0, \tag{5}$$

where ξ_i is an external force on the solid. The solid must also satisfy the equations of equilibrium at its surface,

$$\sigma_{ij}n_j=T_i^n, \tag{6}$$

where n is the exterior normal, and T^n is the external force acting on the unit area surface element with normal n. As the strains e_{ij} are not independent but are linked via the displacements of the elastic body, they must also satisfy the equations of compatibility:

$$\partial_k\partial_l e_{ij}+\partial_i\partial_j e_{kl}=\partial_j\partial_l e_{ik}+\partial_i\partial_k e_{jl}. \tag{7}$$

Equations (5)–(7) along with the stress-strain relationships (4) give us a system of equations, which are sufficient for the complete determination of the equilibrium stress and strain in an elastic body.

For the system we study, external body forces (e.g., gravity) are neglected. Hence Eq. (5) becomes

$$\partial_j\sigma_{ij}=0 \quad \text{for} \quad y<h(x). \tag{8}$$

Our system has periodic boundary conditions in the x direction and is infinite in the negative y direction. We shall assume that the forces on the upper surface due to surface tension (as given by Marchenko and Parshin[21]) are negligible in comparison to the forces due to the mismatch stress. This assumption is fulfilled as long as $\gamma/R\ll M\varepsilon$, where R is the radius of curvature of the surface and M is the plane strain modulus. For typical values of γ, M, and ε, this condition is satisfied when R is larger than the lattice constant. As typical surface features have length scales of the order of 100 nm this assumption is valid. Hence the boundary conditions are given by

$$\sigma_{ij}n_j=0 \ \text{at} \ y=h(x),$$

$$\sigma_{ij}\to 0 \ \text{when} \ y\to-\infty. \tag{9}$$

We now return to our discussion on the determination of the elastic free energy of both the reference state and the perturbed state. For each value of x, our reference state corresponds locally to a *flat* film of thickness $h(x)$ constrained to have the lateral lattice constant of the substrate, i.e., $F_{el}^{(0)}=\int dx\int_{-\infty}^{h(x)}dy f_v^{(0)}[h(x),y]$, where $f_v^{(0)}[h(x),y]$ is the elastic free-energy density of a flat film of thickness $h(x)$ with the

substrate lateral lattice constant. We calculate the correction to the elastic free energy of the perturbed state, δF_{el}, using linear elasticity theory.

When looking at the stability of a strained flat film of thickness C, the obvious first choice for a reference state is that of a flat film of thickness C constrained to have the lateral lattice constant of the substrate. For later calculations we must fully define the reference state and hence need to know its stress $\sigma_{ij}^{(0)}(C,y)$ and free-energy density $f_v^{(0)}(C,y)$. One simple approach to calculate these quantities would be to use linear elasticity with the unstressed film as a reference state. In linear elasticity a flat film of any thickness constrained to have the substrate lateral lattice constant and free to move in the y direction is in equilibrium and has the elastic free-energy density of an infinitely strained film. Hence such a calculation does not predict any C or y dependence in $\sigma_{ij}^{(0)}$ and $f_v^{(0)}$, except for a step function at the film-substrate interface. For example, in the case of plane strain where the mismatch strain is uniaxial (i.e., $e_{xz}=e_{yz}=e_{zz}=0, e_{xy}=0, e_{xx}=\varepsilon$), linear elasticity gives $\sigma_{ij}^{(0)}=M\varepsilon$ and $f_v^{(0)}=M\varepsilon^2/2$, where M is the plane strain modulus. Therefore, variation of the elastic free energy and stress of a flat film with film height is a nonlinear phenomenon, and a model outside of linear elasticity theory must be used to calculate them. As will be shown in Sec. III, small variations in the reference free-energy density with film thickness are crucial in predicting wetting-layer thickness, and a reference free-energy density which has no variation with film thickness will lead to thin films that have no wetting layer.

The disadvantage of our choice of the reference state is that the dependence of h on x leads to lateral variations of the reference state. As a result, the reference stress does not satisfy the condition of mechanical equilibrium. However, the needed corrections vanish in the limit $a/\lambda \to 0$, where a is the length scale over which stress varies in the y direction and λ is the lateral length of typical surface structures. This is because in this limit there are no lateral variations in the reference stress. As typical experimental islands have $\lambda \sim 100$ nm, and as a is of the order of the lattice constant (see below), the corrections to the reference stress are small and have been ignored.

Though linear elasticity cannot be used to calculate properties associated with the reference state, it can still be used to find the correction to the elastic free energy of the perturbed state, δF_{el}. For convenience we work in terms of the reference elastic free energy per unit length in the x direction, $f_{el}^{(0)}[h(x)] \equiv \int_{-\infty}^{h(x)} dy f_v^{(0)}[h(x),y]$, instead of the free energy per unit volume. According to linear elasticity theory, $\delta F_{el} = \int dx \int_{-\infty}^{h(x)} dy [\sigma_{ij}^{(0)} e_{ij} + \frac{1}{2} c_{ijkl} e_{ij} e_{kl}]$. In terms of the stress tensor, we find

$$F_{el} = \int dx\, f_{el}^{(0)} + \int dx \int_{-\infty}^{h(x)} dy \left[\frac{1}{2} S_{ijkl} \sigma_{ij} \sigma_{kl} - \frac{1}{2} S_{ijkl} \sigma_{ij}^{(0)} \sigma_{kl}^{(0)} \right], \tag{10}$$

where we have used the inverted Hooke's law $e_{ij} = S_{ijkl}[\sigma_{kl} - \sigma_{kl}^{(0)}]$. S_{ijkl} are the compliance coefficients of the material.

Using Eqs. (3) and (10) we arrive at an expression for $\delta F/\delta h$:

$$\begin{aligned} \frac{\delta F}{\delta h} = {} & \tilde{\gamma}(\theta)\kappa + \frac{d f_{el}^{(0)}}{dh} \\ & + \left[\frac{1}{2} S_{ijkl} \sigma_{ij} \sigma_{kl} - \frac{1}{2} S_{ijkl} \sigma_{ij}^{(0)} \sigma_{kl}^{(0)} \right] \Bigg|_{y=h(x)} \\ & + \int_{-\infty}^{h(x)} dy \frac{\partial}{\partial h} \left[\frac{1}{2} S_{ijkl} \sigma_{ij} \sigma_{kl} - \frac{1}{2} S_{ijkl} \sigma_{ij}^{(0)} \sigma_{kl}^{(0)} \right], \end{aligned} \tag{11}$$

where κ is surface curvature, θ is the angle between the normal to the surface and the y direction, and $\tilde{\gamma}(\theta) = \gamma(\theta) + \partial^2 \gamma / \partial \theta^2$ is the surface stiffness. The integrand in Eq. (11) is the change in the linear elastic free-energy density as the surface profile changes infinitesimally. Following Sokolnikoff,[20] we now show that this term is of order δh in the absence of external surface or body forces and so can be neglected. When the surface profile changes, the strain in the body changes from e_{ij} to $e_{ij}+e'_{ij}$, where e'_{ij} is of order δh. The elastic free-energy density can be written as $f_v + \Delta f_v = \frac{1}{2} c_{ijkl}(e_{ij}+e'_{ij})(e_{kl}+e'_{kl})$, and the change in elastic free-energy density is $\Delta f_v = c_{ijkl} e_{ij} e'_{kl} + \frac{1}{2} c_{ijkl} e'_{ij} e'_{kl}$. Using Hooke's law (4), the definition of strain, and Eq. (5), we rewrite Δf_v as $\Delta f_v = \partial_j(\sigma_{ij} u'_i) + \xi_i u'_i + \frac{1}{2} c_{ijkl} e'_{ij} e'_{kl}$. The total change in the elastic free energy is $\int \Delta f_v dx dy = \int T_i^n u'_i ds + \int \xi_i u'_i dx dy + \int \frac{1}{2} c_{ijkl} e'_{ij} e'_{kl} dx dy$, where the first term on the right-hand side is an integral over the film surface. To obtain this we used Eq. (6). In the absence of external surface or body forces the first two terms on the right-hand side of the above equation vanish, and we are left with the equation $\int \Delta f_v dx dy = \int \frac{1}{2} c_{ijkl} e'_{ij} e'_{kl} dx dy$. e'_{ij} is of order δh, and hence the integrand in Eq. (11), $\Delta f_v / \delta h$, is of order δh. Therefore the last term in Eq. (11) can be ignored for infinitesimal changes to the solid surface and we have

$$\frac{\delta F}{\delta h} = \tilde{\gamma}\kappa + \frac{d f_{el}^{(0)}}{dh} + \left\{ \frac{1}{2} S_{ijkl} \sigma_{ij} \sigma_{kl} - \frac{1}{2} S_{ijkl} \sigma_{ij}^{(0)} \sigma_{kl}^{(0)} \right] \Bigg|_{y=h(x)}. \tag{12}$$

As the above equation gives $\delta F/\delta h$ at the solid surface, all variables in the equation are also given at the surface. In particular $\sigma_{ij}^{(0)}(h, y=h)$ is taken as the stress at the surface of a flat solid of height $h(x)$ and hence must vanish when $h \leqslant 0$, since then the film is absent. $d f_{el}^{(0)}(h)/dh$ is determined by calculating how the reference elastic free energy of the solid changes as monolayers are added to the solid surface. When $h \leqslant 0$, $d f_{el}^{(0)}/dh = 0$, as the substrate is completely relaxed. In principle, Eq. (12) should also contain derivatives of γ with respect to h. However, we believe that the variation of surface tension with h away from a step dependence is due to elastic effects. Since we included all elastic contributions

in the zero-strain elastic free energy, we modeled γ as a step function, taking the value of the substrate surface tension for $h \leqslant 0$ and the film surface tension for $h > 0$. Thus all partial derivatives of γ with respect to surface height vanish and were omitted from Eq. (12).

Equations (2) and (12) form a complete model of surface evolution. In order to solve this model, the chemical potential [given by Eq. (12)] for a given surface must be found, and so the linear elastic free-energy density at the solid surface, $f_v^{lin} = \frac{1}{2} S_{ijkl}\sigma_{ij}\sigma_{kl}|_{y=h(x)}$ must be calculated. For an isotropic solid under plane strain with zero force boundary conditions the above expression simplifies considerably to give $f_v^{lin} = (\sigma_{xx}+\sigma_{yy})^2|_{y=h(x)}/2M$, where M is the plane strain modulus. Hence we must determine the stress at the surface of the film. This is done by finding the stress which satisfies both the linear elasticity equations [the equations of compatibility (7) and equilibrium (8)] and the boundary conditions (9).

For an isotropic solid under plane strain, finding the stress which satisfies the linear elasticity equations and the boundary conditions can be reduced to finding the stress function, W, which satisfies the boundary conditions (9) and the biharmonic equation (see, e.g., Timoshenko and Goodier[22] or Mikhlin[23]):

$$\Delta^2 W = \Delta(\Delta W) = \frac{\partial^4 W}{\partial x^4} + 2\frac{\partial^4 W}{\partial x^2 \partial y^2} + \frac{\partial^4 W}{\partial y^4} = 0, \quad (13)$$

with $\sigma_{xx} = \partial^2 W/\partial y^2$, $\sigma_{xy} = -\partial^2 W/\partial x \partial y$, and $\sigma_{yy} = \partial^2 W/\partial x^2$.

In order to model the early evolution of faceted islands, and to study the effect of an anisotropic form of surface tension on the wetting layer, we used the cusped form of surface tension given by Bonzel and Preuss,[24] which shows faceting in a free crystal: $\gamma(\theta) = \gamma_0\{1+\beta|\sin[\pi\theta/(2\theta_0)]|\}$, where $\beta \approx 0.05$ and θ_0 is the angle of maximum γ. The value of γ_0 was taken as 1 J/m^2 in the substrate and about 75% of that in the film (as is the case for Ge/Si). This ensures a wetting layer of at least one monolayer. We considered a crystal which facets at 0°, ±45°, and ±90° with $\theta_0 = \pi/8$. The cusp gives rise to $\tilde{\gamma} = \infty$. However, a slight miscut of the low-index surface along the z direction leads to a rounding of the cusp, which can be described by

$$\gamma(\theta) = \gamma_0\left[1 + \beta\sqrt{\sin^2\left(\frac{\pi}{2\theta_0}\theta\right) + G^{-2}}\right], \quad (14)$$

where, for example, $G = 500$ corresponds to a miscut angle, $\Delta\theta \approx 0.1°$. As mentioned earlier all the results in this paper relate to surfaces with a very small miscut angle in the z direction.

III. LINEAR STABILITY ANALYSIS

In this section we carry out a linear stability analysis of Eq. (2) against a sinusoidal perturbation of wave number k, similar to that carried out in Ref. 25 for an infinitely thick stressed film. We thus look for a height profile of the form $h(x,t) = C + \delta(t)\sin kx$, which solves Eq. (2) to first order in δ. To calculate the linear elastic energy we find the solutions of Eq. (13), which satisfy the boundary conditions (9). $\sigma_{xy}^{(0)}$ vanishes because the film is hydrostatically strained, and $\sigma_{yy}^{(0)} = 0$ since in the reference state the force perpendicular to the surface vanishes. Hence the only nonzero component of the reference stress is $\sigma_{xx}^{(0)}(h,y)$. Stress functions of the form

$$W = \sigma_{xx}^{(0)}(h,y)y^2/2 + (A+By)e^{ky}\sin(kx) \quad (15)$$

satisfy the biharmonic equation. This gives stresses of the form

$$\sigma_{xx} = k[2B + (A+By)k]e^{ky}\sin(kx) + \sigma_{xx}^{(0)}(h,y),$$

$$\sigma_{yy} = -k^2(A+By)e^{ky}\sin(kx),$$

$$\sigma_{xy} = -k[B+(A+By)k]e^{ky}\cos(kx).$$

To first order in δ the stresses that satisfy the biharmonic equation and the boundary conditions are given by

$$\sigma_{xx} = -\delta k e^{-kC}\sigma_{xx}^{(0)}(C,C)[2+(y-C)k]e^{ky}\sin(kx) + \sigma_{xx}^{(0)}(h,y),$$

$$\sigma_{yy} = \delta k^2 e^{-kC}\sigma_{xx}^{(0)}(C,C)(y-C)e^{ky}\sin(kx),$$

$$\sigma_{xy} = \delta k e^{-kC}\sigma_{xx}^{(0)}(C,C)[1+(y-C)k]e^{ky}\cos(kx).$$

At the surface these stresses take the forms

$$\sigma_{xx} = -2\,\delta k\sigma_{xx}^{(0)}(C,C)\sin(kx) + \sigma_{xx}^{(0)}(C,C) + \delta\sin(kx)d\sigma_{xx}^{(0)}/dh|_{h=C},$$

$$\sigma_{yy} = 0,$$

$$\sigma_{xy} = \delta k\sigma_{xx}^{(0)}(C,C)\cos(kx).$$

Note that all the derivatives in the Taylor expansions used in this analysis are with respect to h, the reference film thickness and not with respect to y, the depth within the reference film. This is because in calculating the chemical potential we are interested in how the free energy of the film changes as material is added or removed from the film surface, i.e., how the free-energy of the film changes as the film thickness changes and not how the free energy density of the film varies within the film.

Using the above stresses in Eq. (12), we obtain the expression

$$\frac{\delta F}{\delta h} = \tilde{\gamma}\kappa + \frac{df_{el}^{(0)}}{dh} + \frac{1}{2M}(\sigma_{xx}+\sigma_{yy})^2 - \frac{1}{2M}(\sigma_{xx}^{(0)}+\sigma_{yy}^{(0)})^2 = \delta\sin(kx)\left\{\frac{d^2 f_{el}^{(0)}}{dh^2} - 2k\frac{[\sigma_{xx}^{(0)}(C,C)]^2}{M} + \tilde{\gamma}_0 k^2\right\} + \frac{df_{el}^{(0)}}{dh}(C,C), \quad (16)$$

where $\tilde{\gamma}_0=\tilde{\gamma}(\theta=0)$. Combining the above equation with the evolution Eq. (2) gives the following equation for $\delta(t)$:

$$\frac{d\delta}{dt}=Kk^2\left\{-k^2\tilde{\gamma}_0+2k\frac{[\sigma_{xx}^{(0)}(C,C)]^2}{M}-\frac{d^2f_{el}^{(0)}}{dh^2}\right\}_{h=C}\delta, \quad (17)$$

where $K=D_s\eta\Omega^2/k_BT$. Each term in the brackets in this equation has a simple physical significance. The first term is a surface-tension term. Surface tension acts to reduce surface curvature, κ, and so this term is negative, thereby reducing the perturbation amplitude, and is linear in $\kappa\sim k^2$. The second term in this equation is a mismatch stress term. Regions of high stress have large chemical potential, and so atoms tend to detach from these regions and attach to regions of small chemical potential. In a mismatch stressed solid, valleys or cusps are regions of high stress, hence material moves from the valleys to the hills of a perturbed surface increasing perturbation amplitude. The contribution of this term is propotional to the density of valleys, which is linear in k. The last term is a reference state term. If $d^2f_{el}^{(0)}/dh^2>0$ it costs more energy to add a monolayer to a flat film than is gained by removing a monolayer, and hence it costs energy to perturb a film. Thus, positive $d^2f_{el}^{(0)}/dh^2$ stabilizes a flat thin film, whereas negative $d^2f_{el}^{(0)}/dh^2$ leads to an instability. Obviously this reference state term is present even if the film is flat and hence is independent of k.

Equation (17) implies that the flat film is stable at all perturbation wavelengths as long as

$$\frac{[\sigma_{xx}^{(0)}(C,C)]^4}{M^2}\leqslant\tilde{\gamma}_0\frac{d^2f_{el}^{(0)}}{dh^2}\bigg|_{h=C}, \quad (18)$$

and the equality holds at the critical wetting-layer thickness, where perturbations of wave number $k=[\sigma_{xx}^{(0)}(C,C)]^2/(M\tilde{\gamma}_0)$ are marginal. $\tilde{\gamma}_0$ is positive if $\theta=0$ is a surface seen in the equilibrium free crystal.[26] As mentioned earlier, $\tilde{\gamma}_0\rightarrow\infty$ at a perfect facet and is large and positive on a surface with a small miscut, as is the case for most of the materials used in epitaxial films. Therefore, a linearly stable wetting layer of finite thickness can exist only if $d^2f_{el}^{(0)}/dh^2>0$. Note that for the wetting layer to have a finite rather than an infinite thickness, $d^2f_{el}^{(0)}/dh^2$ must decrease to a value less than the left-hand side of Eq. (18) as the thickness of the film increases. $\sigma_{xx}^{(0)}(C,C)$ depends linearly on the lattice mismatch ε, and hence the left-hand side of Eq. (18) is proportional to ε^4, while the right-hand side of Eq. (18) is proportional to ε^2 due to the dependence of $f_{el}^{(0)}$ on lattice mismatch. Therefore, if $d^2f_{el}^{(0)}/dh^2>0$, the thickness of the wetting layer increases with decreasing lattice mismatch and diverges in the limit $\varepsilon\rightarrow0$.

Note that the maximum thickness of a flat film which is stable to infinitesimal perturbations is given by Eq. (18) when the equality holds. A film slightly thicker is unstable to perturbations of wavelength $\lambda=2\pi M\tilde{\gamma}_0/[\sigma_{xx}^{(0)}(C,C)]^2$. For films which are nearly perfect facets with small miscut angles these wavelengths are larger than the typical sample size and so practically such perturbations will never occur. However as will be explained in Sec. V, the film can be nonlinearly unstable to smaller-wavelength perturbations of a nonzero amplitude at physically reasonable wavelengths. Hence the inequality in Eq. (18) is only useful in predicting the stability of films with large miscut angles or above the roughening temperature. At small miscut angles the stability of the film to large perturbations will predict its maximum thickness. This issue is discussed in more detail in Sec. V.

IV. CALCULATION OF THE NONLINEAR ELASTIC FREE ENERGY OF A FLAT FILM

As can be seen from both Eq. (12) and Eq. (18), the dependence of the nonlinear elastic free energy of a flat film $f_{el}^{(0)}(h)$ on film thickness, h, is vital in order to determine both wetting-layer thickness and thin-film evolution. This free energy depends strongly on the mismatch stress $\sigma_{ij}^{(0)}$, and its dependence on the y coordinate. As a result of the sharp interface between the substrate and the film, we expect $\sigma_{ij}^{(0)}$ to behave as a step function of y with small corrections due to elastic relaxation. If we ignore these small corrections, the resulting free energy $f_{el}^{(0)}(h)$ is proportional to film thickness, and its second derivative vanishes. Hence according to Eq. (18), the thickness of the critical wetting layer vanishes. The correction due to elastic relaxation is therefore extremely important. As discussed earlier, this correction vanishes within linear elasticity theory. This led some investigators[27] to claim that the variation in free energy over the interface was due to nonelastic effects, e.g., film-substrate material mixing over the interface. However, we claim that this is not necessary, since nonlinear elasticity can explain the corrections to the step-function form of the free energy.

The nonlinear elastic free energy of the reference state, $f_{el}^{(0)}(h)$, is calculated for a solid with a flat surface of height h. Hence in order to calculate $df_{el}^{(0)}/dh$, we determine $f_{el}^{(0)}$ for flat solids of heights $h+\delta/2$ and $h-\delta/2$, and use the estimate $df_{el}^{(0)}/dh=[f_{el}^{(0)}(h+\delta/2)-f_{el}^{(0)}(h-\delta/2)]/\delta$. Ideally, first-principles, substance-specific calculations should be performed in order to evaluate $\sigma_{xx}^{(0)}(h,y)$ and $f_{el}^{(0)}(h)$, and we intend to carry out such calculations. However, the qualitative general behavior of $f_{el}^{(0)}(h)$ can be obtained from much simpler models which have the advantage of being able to separate universal elastic effects from substance-specific effects due to the different types of bonds present at the interface of a real system. We calculated $\sigma_{xx}^{(0)}(h,y)$ and $f_{el}^{(0)}(h)$ for two-dimensional networks of balls and springs of varying lattice type and spring constants. In these calculations δ is one monolayer, and $f_{el}^{(0)}(h)$ is calculated at film thicknesses of integer numbers of monolayers from no film up to 10 monolayers of film. Values of $f_{el}^{(0)}(h)$ for film heights of fractional monolayers are interprolated from the values calculated at integer monolayer heights.

In the ball-and-spring model the balls are connected by springs that obey Hooke's law. Note that this does not imply that the stress-strain relationship of the ball-and-spring network is linear (a discussion of this point can be found in Ref.

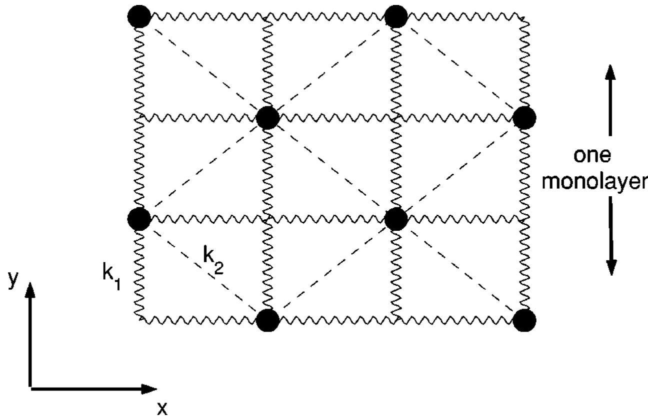

FIG. 2. Example of a fcc-like lattice. The circles represent balls. The curvy lines are springs of spring constant k_1, and the dashed lines represent springs of spring constant k_2.

28). The natural spring length has a step variation over the interface, and the balls are placed on a lattice with the substrate lattice constant. Thus balls in the substrate are connected by springs of their natural length, whereas balls in the film are connected by springs that have undergone a hydrostatic transformation strain and have length larger than their natural length by a factor of $1+e$, where e is the homogeneous strain in the film. The network was then allowed to relax, with the film free to move in the y direction, and periodic boundary conditions were applied in the x direction to ensure that the system boundaries in this direction were fixed to the natural substrate length.

We calculated the mismatch stress $\sigma_{xx}^{(0)}$ within the relaxed film and at the film surface. We also calculated the dependence of mismatch surface stress $\sigma_{xx}^{(0)}(h,h)$ and the nonlinear elastic free energy $f_{el}^{(0)}(h)$ on varying film thicknesses, h. We carried out these calculations for various two-dimensional networks of balls and springs with varying spring constants. An example of the ball-and-spring model on a fcc-like lattice is shown in Fig. 2.

Simulations showed that while individual atoms were free to move in the x direction, they actually moved only in the y direction. The relaxation in the y direction depended on the film thickness and on the depth of the atom in the lattice but was independent of x. In general balls at depth of more than 3 ML into the substrate experienced no stress. The stress experienced by balls close to the interface depended on the lattice type, spring constants, and ball position within the monolayer. A few monolayers into the film, balls experienced the stress of an infinite thickness film, $M\varepsilon$. At the film surface balls showed large relaxation. Figure 3 shows an example of the mismatch stress, $\sigma_{xx}^{(0)}(h,y)$, in a typical fcc-like lattice.

Note that the springs in a simple square lattice could relax completely in the y direction. Therefore, for such a lattice the relaxation is independent of spring depth within the film or film thickness, and $f_{el}^{(0)}(h)$ varies linearly with film thickness. Hence for a square lattice $d^2 f_{el}^{(0)}(h)/dh^2=0$. Only when diagonal bonds, such as those in a fcc lattice, were present did the springs show depth-dependent relaxation

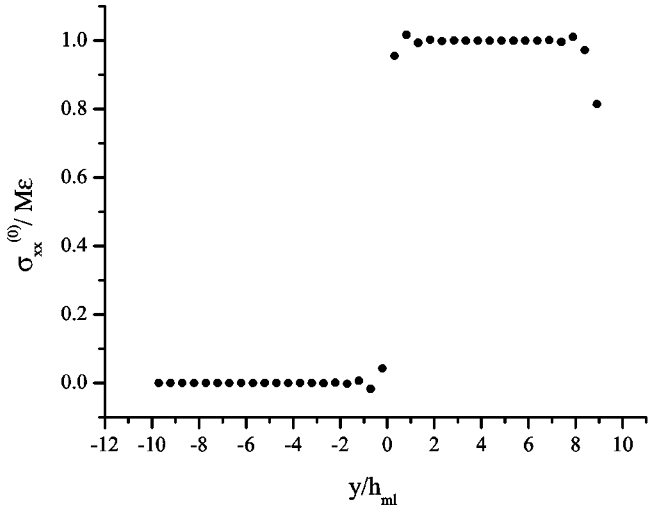

FIG. 3. Mismatch-induced stress, $\sigma_{xx}^{(0)}(h,y)/M\varepsilon$, in a typical fcc-like lattice. The film is 8-ML thick and the substrate is 10-ML thick. h_{ml} is the thickness of one monolayer.

such as that described above. The inability of the springs to completely relax due to the presence of diagonal bonds was a necessary condition for $f_{el}^{(0)}(h)$ to vary nonlinearly with film height. In such incompletely relaxed films the nonlinear dependence of $f_{el}^{(0)}$ on h arises from the elastic relaxation at the surface and its coupling to the relaxation at the film-substrate interface. A similar effect should occur in real systems due to surface reconstruction, for example.

A typical behavior of $df_{el}^{(0)}/dh$ is shown in Fig. 4, where it is seen that $f_{el}^{(0)}(h)$ indeed depends on the thickness h. Moreover, the model predicts that $d^2 f_{el}^{(0)}/dh^2>0$ and decreases with increasing film thickness, and therefore according to the inequality (18) and the discussion following it, there should be a linearly stable wetting layer, whose thickness is finite and increases with decreasing lattice mismatch.

While the detailed dependence of $df_{el}^{(0)}(h)/dh$ on film

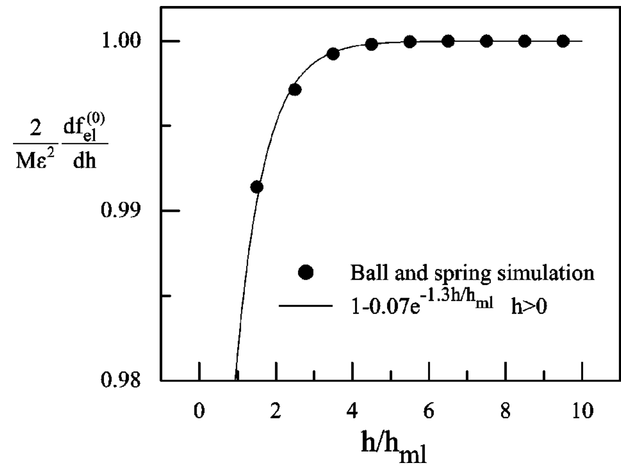

FIG. 4. Variation with film thickness of the elastic free energy of a relaxed ball-and-spring system, $df_{el}^{(0)}/dh$, as a function of film thickness h. The free energy is normalized to the infinite film linear elastic energy density, $\frac{1}{2}M\varepsilon^2$. h_{ml} is the thickness of one monolayer.

thickness close to the substrate-film interface [$\leqslant 3$ ML] varied between different networks, it showed the same general behavior. In all systems $d^2 f_{el}^{(0)}(h)/dh^2$ showed exponential decay with a decay length of about a monolayer from the interface. The dimensionless quantity $(2/M\varepsilon^2)(df_{el}^{(0)}/dh)$ was independent of lattice mismatch sign or magnitude. $df_{el}^{(0)}/dh$ increased with film thickness. As the film thickness increases $df_{el}^{(0)}/dh$ asymptotically approaches the elastic free-energy density of an infinite film, $M\varepsilon^2/2$, as expected.

The results of both Tersoff[13] and Wang *et al.*[15] show similar behavior suggesting that the fundamental form of $f_{el}^{(0)}(h)$ which gives rise to the wetting layer is due to universal elastic effects and that the specifics of the system only change the details of how thick that wetting layer will be.

We can explain the increase of $df_{el}^{(0)}/dh$ with film thickness intuitively. $df_{el}^{(0)}/dh$ is the change in the free energy of a film as a monolayer is added. When a monolayer is added to a thick film the contribution to the free energy from the surface atoms and the interface remains the same and the energy added is effectively that of a monolayer in the "bulk" of the film. Atoms in the bulk of a thick film are more constrained than those in a thin film where the atoms are relatively free to move and relax. When a monolayer is added to a thin film the energy change is in between that of the constrained thick-film bulk atoms and the relaxed surface atoms. Hence more free energy is needed to add a monolayer to a thick film and $df_{el}^{(0)}/dh$ increases with film thickness.

For the calculations used later in this paper we used the function

$$df_{el}^{(0)}(h)/dh = \frac{M\varepsilon^2}{2}[1-0.05\exp(-h/h_{ml})] \quad \text{for} \quad h>0, \tag{19}$$

and $df_{el}^{(0)}(h)/dh=0$ for $h\leqslant 0$. h_{ml} is the thickness of one monolayer. In previous works[11,12,27] on the physics of the wetting layer it was assumed that the reference state energy variation is a smooth function of h, mainly in order to avoid nonanalyticities at the interface. In contrast, our reference state energy variation behaves as a step function of the surface height with a small but important correction.

The deviations in the mismatch stress (averaged over the surface monolayer) at the film surface $\sigma_{xx}^{(0)}(h,h)$ from a step function, $\sigma_{xx}^{(0)}(h,h)=M\varepsilon$ when $h>0$, was shown to be small ($<5\%$) but dependent on spring constants and lattice type (see Fig. 5). As variations in $\sigma_{xx}^{(0)}(h,h)$ only slightly alter the wetting-layer thickness predicted from Eq. (18), we decided to use the step-function form of mismatch stress.

Combining the behavior of $df_{el}^{(0)}/dh$ from Eq. (19) with the inequality (18), we obtained an expression for the linear stability wetting-layer thickness, h_c:

$$h_c/h_{ml} = \max\{1, \ln[\tilde{\gamma}_0/(40M\varepsilon^2 h_{ml})]\}. \tag{20}$$

Thus, the wetting-layer thickness increases with decreasing lattice mismatch, as observed in experiments.

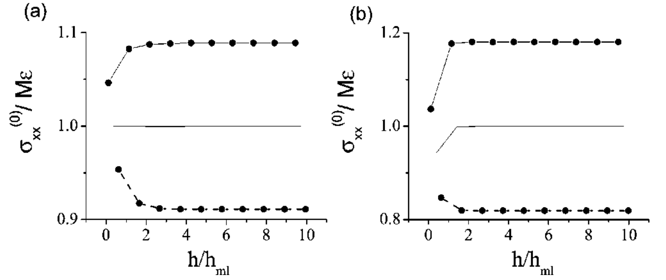

FIG. 5. Variation of mismatch-induced stress at the film surface, $\sigma_{xx}^{(0)}(h,h)/M\varepsilon$, for varying film thickness, h. The lattice is fcc-like (see Fig. 2). The dashed lines with circles denote $\sigma_{xx}^{(0)}/M\varepsilon$ of atoms at the top of a monolayer. The solid lines with circles denote $\sigma_{xx}^{(0)}/M\varepsilon$ of atoms at the bottom of a monolayer. The solid lines without circles represent the averages of $\sigma_{xx}^{(0)}/M\varepsilon$ over a monolayer. The spring constants which were used are (a) $k_1=1$ and $k_2=1$ and (b) $k_1=1$ and $k_2=5$.

V. NUMERICAL SIMULATIONS OF THIN-FILM GROWTH

As explained at the end of Sec. III, for systems with small mismatch and/or small vicinality (miscut angle) one has to go beyond linear stability in order to understand their evolution. To this end we carried out numerical simulations of the evolution of the strained film. The evolution Eq. (2) given by Mullins,[19] which is derived from the Nernst-Einstein relation (1), includes derivatives of the chemical potential, μ, along the surface. This chemical potential is defined as the change in free energy when an atom is added to the surface. Continuum theory assumes that the free-energy change when the surface is changed by an infinitesimal amount is proportional to this chemical potential ($\mu=\Omega\,\delta F/\delta h$). However, when we solved the evolution equation by directly calculating the chemical potential from Eq. (12) at points along the film surface we experienced numerical instabilities.

We have come up with the following solution to this problem. The Nernst-Einstein equation can be derived by considering material of atomic volume moving along the solid surface. When material jumps between neighboring atomic sites, it must cross a free-energy barrier of $\Delta F_{\pm}=E_d+(F_{\pm}-F_0)/2$, where E_d is the potential barrier for diffusion, $F_{\pm}$ is the free energy of the film after material has been moved, and F_0 is the free energy of the film before material is moved. The positive and negative signs stand for forward and backward jumps, respectively. This leads to the following equation for material velocity along the surface:

$$\begin{aligned} v &= \omega a e^{-E_d/k_BT}[e^{-(F_+-F_0)/2k_BT} - e^{-(F_--F_0)/2k_BT}] \\ &= \frac{D_s}{a}[e^{-(F_+-F_0)/2k_BT} - e^{-(F_--F_0)/2k_BT}], \end{aligned} \tag{21}$$

where ω is the attempt rate and a is the jump length. When (F_+-F_0) and (F_--F_0) are small, this equation gives the Nernst-Einstein relation (1).

We solved Eq. (21) using the following numerical scheme. For every two adjacent points on the surface, the surface height of the left point was changed by $\pm\delta h$ and of the right point by $\mp\delta h$ so as to give a transfer of material of

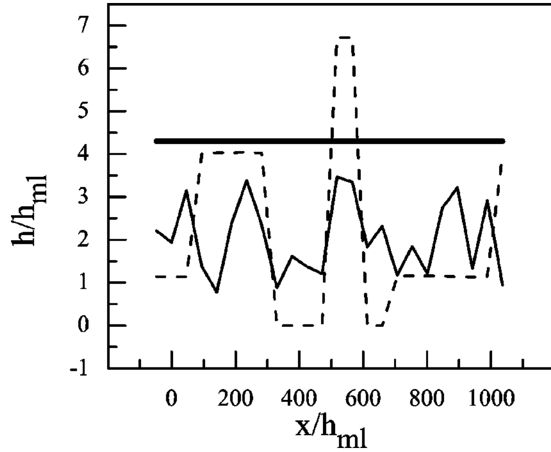

FIG. 6. Evolution of a randomly perturbed film, in which perturbations were larger than the critical perturbation amplitude. Lattice mismatch in this film is 4%. The initial film surface is shown as a thin solid line. The dashed line shows the film surface at a later time. The linear wetting-layer thickness is shown as a thick solid line.

atomic volume backwards and forwards along the surface, respectively. The change in surface free energy, $\int dx\, \gamma\sqrt{1+(\partial h/\partial x)^2}$, was calculated for this material transfer. The change in the elastic free energy was calculated at each point using the integral of Eq. (12), $\delta F = \pm\{(df_{el}^{(0)}/dh)+[\frac{1}{2}S_{ijkl}\sigma_{ij}\sigma_{kl}-\frac{1}{2}S_{ijkl}\sigma_{ij}^{(0)}\sigma_{kl}^{(0)}]|_{y=h(x)}\}\delta h$. The linear elastic energy was calculated by solving the biharmonic Eq. (13) with the boundary conditions (9). This was done by solving a boundary integral equation in terms of the complex Goursat functions, the details of which can be found in the paper of Spencer and Meiron.[29]

The stability of thin films

According to Eq. (20), anisotropic surface tension greatly enlarges the linearly stable wetting-layer thickness. Does this conclusion survive beyond linear stability analysis? When a linearly stable flat film is perturbed strongly so that the surface orientation in some regions is far from the $\theta=0$ direction, the local surface stiffness in these regions is much smaller than the $\theta=0$ stiffness. This tends to destabilize the linearly stable film. Indeed, we carried out numerical simulations (using the procedure described above) that showed that films thinner than the linear wetting layer were unstable to perturbations greater than a certain critical amplitude (see Fig. 6). Hence films thinner than the linear wetting-layer thickness are *metastable*. When large perturbations were applied, faceted islands developed in the film, which underwent ripening at later stages of the evolution.

We carried out simulations for films perturbed by random perturbations and by perturbations of a single wavelength. The critical perturbation amplitude, δ_c, depends on the wavelength of the perturbation, λ, taking its minimal value

$$\delta_c^m = \min_{\lambda} \delta_c(\lambda) \tag{22}$$

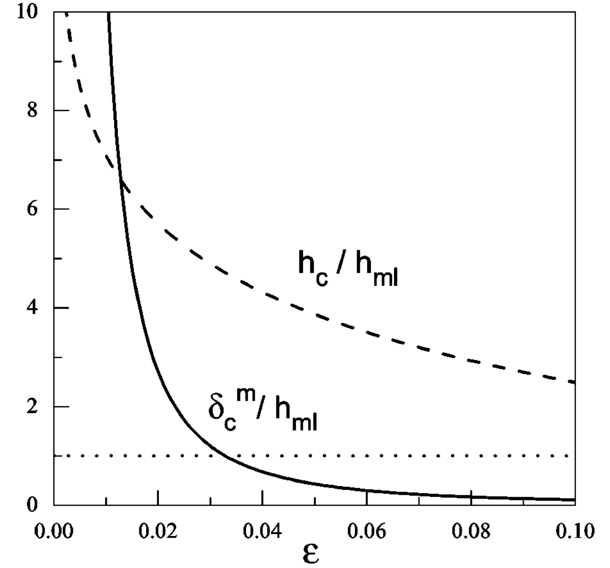

FIG. 7. Variation of the minimal critical perturbation amplitude, δ_c^m, and linear wetting-layer thickness, h_c, with lattice mismatch, ε. The minimal critical perturbation amplitude, δ_c^m/h_{ml}, is represented by the solid line. The linear wetting-layer thickness, h_c/h_{ml}, is represented by the dashed line. The dotted line shows the size of one monolayer, h_{ml}, for comparison.

at $\lambda/l_o \sim 10-50$, where $l_o = 2\gamma_o/M\varepsilon^2$. δ_c^m in monolayers is plotted as a function of lattice mismatch in Fig. 7. The linear wetting-layer thickness for $G=500$, $M=1.5\times10^{11}$ N/m^2, and $h_{ml}=5$ Å is also shown for comparison.

δ_c^m was found to be proportional to ε^{-2}. The ε^{-2} dependence is expected for an infinite film as in this case the evolution equations [Eq. (2) together with Eq. (12)] can be made spatially dimensionless by scaling all lengths by l_0. Hence all perturbations of size δ/l_0 and with the same dimensionless wave number kl_0 will evolve identically.

δ_c^m was largely independent of cusp smoothness G, unlike the linear wetting-layer thickness which depended strongly on G. The evolution of a large perturbation was identical for $G\rightarrow\infty$ and a perfect cusp in the surface tension, whereas Long *et al.*[30] showed that the linear stability analysis for the two cases predicted very different evolution. Both these observations suggest that unlike the linear wetting-layer thickness the critical perturbation amplitude can be used in predicting the outcome of experimental thin-film growth. The mean-square amplitude of the random perturbation needed to destabilize thin films was also shown to be largely independent of G and was proportional to ε^{-2}.

When the lattice mismatch is small, δ_c^m is much larger than the linear wetting-layer thickness (see Fig. 7). Hence, flat films thinner than the linear critical thickness are stable at small lattice mismatch. As the linear critical thickness at small lattice mismatch is very large, we expect the film to first become unstable to misfit dislocations. This is indeed seen in experiments.[8,9]

At intermediate lattice mismatch, δ_c^m is of the order of a few monolayers. Hence we expect such a film to become unstable as perturbations of this amplitude are physically likely. In this regime films should develop growing perturba-

tions at wavelengths given by $\lambda/l_o \sim 10-50$. This corresponds to wavelengths of a few hundred nanometers. This typical wavelength decreases as lattice mismatch increases, agreeing with experiment.[6,8] As ε increases, δ_c^m decreases in this regime from about 10 ML to approximately 1 ML, and we expect the thickness of the film needed to support such perturbations to correspondingly decrease. Such a trend is seen in experiments.[6–9] In order to compare quantitative wetting-layer thickness and its lattice mismatch dependence with experiments we will have to carry out first-principles, substance-specific calculations to evaluate $f_{el}^{(0)}(h)$. However, the general qualitative trends predicted here agree with experimental observations.

Looking at Fig. 7 we see that at intermediate lattice mismatch the critical perturbation amplitude, δ_c^m, and the linear wetting-layer thickness are of the same order of magnitude (several monolayers). This could mean that we have to also consider the linear wetting-layer thickness with its strong dependence on the surface miscut angle when deciding whether or not a thin film will be unstable. However, the infinitesimal perturbations needed to perturb the linear wetting layer occur at wavelength $\lambda = (2\pi/M\varepsilon^2)\tilde{\gamma}_0$, whereas the typical wavelength at which critical amplitude perturbations first appear in the film is $\lambda \sim 10(2/M\varepsilon^2)\gamma_0$. Using expression (14), the ratio between these two wavelengths is approximately equal to G. For physical values of G the linear wetting-layer perturbations will have wavelengths of the order of 100 μm which is larger than the typical sample size, whereas the wavelength which corresponds to the minimal critical perturbation is much smaller ($\sim$100 nm). Therefore, physical thin films should first become unstable when the film thickness is large enough to support perturbations larger than the critical perturbation amplitude.

For very large mismatch, a perturbation smaller than a monolayer is sufficient in order to destabilize the linearly stable wetting layer. Therefore, in practice, the wetting layer is a single monolayer in this case.

VI. EARLY EVOLUTION OF THIN FILMS WITH MATERIAL DEPOSITION

We carried out our calculations with two different types of material deposition: The first type is deposition at a steady rate in the vertical y direction, corresponding to any directed deposition (e.g., molecular-beam epitaxy). The evolution Eq. (2) then becomes

$$\frac{\partial h}{\partial t} = \frac{D_s \eta \Omega}{k_B T} \frac{\partial}{\partial x} \frac{\partial \mu}{\partial s} + V_D, \tag{23}$$

where V_D is the material deposition rate.

The second type is deposition, constant in the direction perpendicular to the film surface, corresponding to liquid phase epitaxy, for example. Early growth with this method of deposition has been studied by Chiu and Gao.[11] In this case the evolution equation becomes

$$\frac{\partial h}{\partial t} = \frac{D_s \eta \Omega}{k_B T} \frac{\partial}{\partial x} \frac{\partial \mu}{\partial s} + \frac{V_D}{n_y}, \tag{24}$$

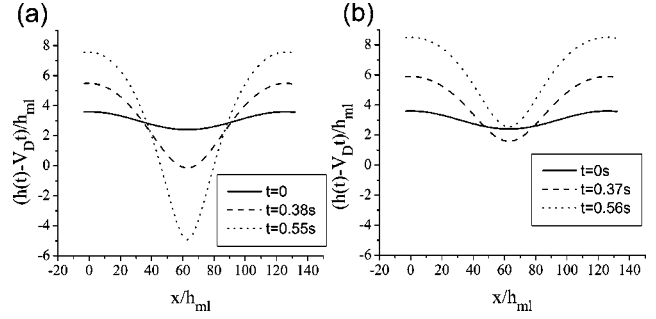

FIG. 8. Film evolution at very high deposition rates ($V_D = 1200$ nm/s) when surface tension is isotropic. $k = 0.75 \times 2M\varepsilon^2/\tilde{\gamma}_0$. (a) Deposition is constant in the vertical y direction. (b) Deposition is constant perpendicular to the film surface.

where n_y is the y component of the normal vector to the surface.

We performed linear stability analysis in order to obtain the analytical early evolution equation of a perturbed thin film. This analysis is valid for both types of material deposition. Under steady deposition, Eq. (17) becomes

$$\frac{d\delta}{dt} = K\left[-k^4\tilde{\gamma}_0 + 2k^3 M\varepsilon^2 - k^2 \frac{d^2 f_{el}^{(0)}(C+V_D t)}{dh^2}\right]\delta, \tag{25}$$

where we have assumed the reference state mismatch stress is given by a step function, $\sigma_{xx}^{(0)}(h,h) = M\varepsilon$ when $h>0$, and $\sigma_{xx}^{(0)}(h,h)=0$ when $h<0$. Using the general form (obtained from the ball-and-spring model) of $d^2 f_{el}^{(0)}/dh^2 \simeq \chi(M\varepsilon^2/2h_{ml})\exp(-h/h_{ml})$, where χ is a constant, gives the following solution for perturbation growth:

$$\delta(t) = \delta_0 \exp(K\{(-k^4\tilde{\gamma}_0 + 2k^3 M\varepsilon^2)t + k^2\chi(M\varepsilon^2/2V_D) \times \exp(-C/h_{ml})[\exp(-V_D t/h_{ml}) - 1]\}). \tag{26}$$

Note that in linear stability analysis a perturbation in an infinite film decays when $k > 2M\varepsilon^2/\tilde{\gamma}_0$ and grows exponentially when $k < 2M\varepsilon^2/\tilde{\gamma}_0$.

For isotropic surface tension, numerical computations showed that when $k^* < k < 2M\varepsilon^2/\tilde{\gamma}_0$, with $k^* \approx 0.875 \times 2M\varepsilon^2/\tilde{\gamma}_0$, both methods of deposition lead to cusp formation in the surface valleys. The cusps initially evolve according to the linear evolution Eq. (26) and then slow and reach a steady-state morphology. Spencer and Meiron[29] observed such steady states in infinitely thick stressed films. However when $k < k^*$, surface evolution depends on the method of material deposition. When deposition is constant in the vertical y direction increasingly sharp cusps form in the surface valleys [see Fig. 8(a)], which continue to grow exponentially. In contrast when deposition is constant perpendicular to the surface at very high deposition rates cusp formation is slowed [see Fig. 8(b)] and the surface shows signs of reaching a steady-state morphology as for $k > k^*$.

This can be seen in Fig. 9. The plot (shown as squares in the figure) starts as a graph of constant positive slope representing an exponentially growing perturbation as predicted

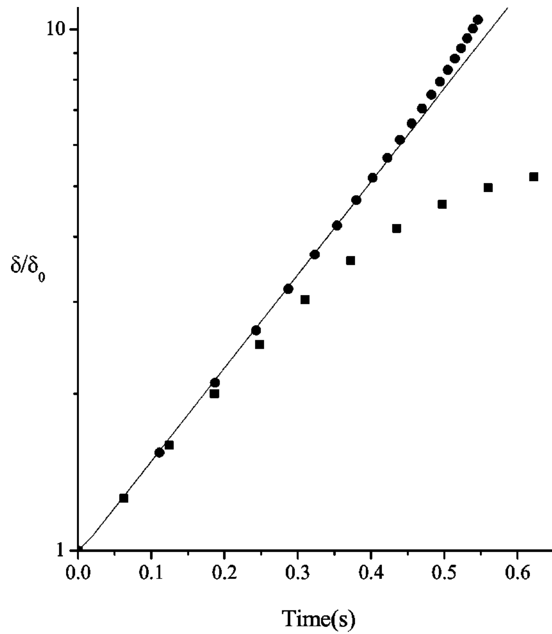

FIG. 9. Film evolution at very high deposition rates ($V_D = 1200$ nm/s) when surface tension is isotropic. The line represents the linear evolution equation, the circles represent the results from the numerical simulation when deposition is constant in the y direction, and the squares represent the results from the numerical simulation when deposition is constant perpendicular to the surface. $k = 0.75\times 2M\varepsilon^2/\tilde{\gamma}_0$. The parameters used here are $D_s = 3.599 \times 10^{-13}$ m^2/s, $\Omega = 1.38\times 10^{-29}$ m^3, $\eta = 1.74\times 10^{19}$ m^{-2}, $T = 700$ K, $k = 10^8$ m^{-1}, $\gamma_0 = \tilde{\gamma}_0 = 1$, $\varepsilon = 2\%$, $M = 1.67\times 10^{11}$, $\chi = 1$, $C = 0.75$ ML, and $h_{ml} = 2$ nm. Note the deviation from the linear stability analysis results when deposition is perpendicular to the surface.

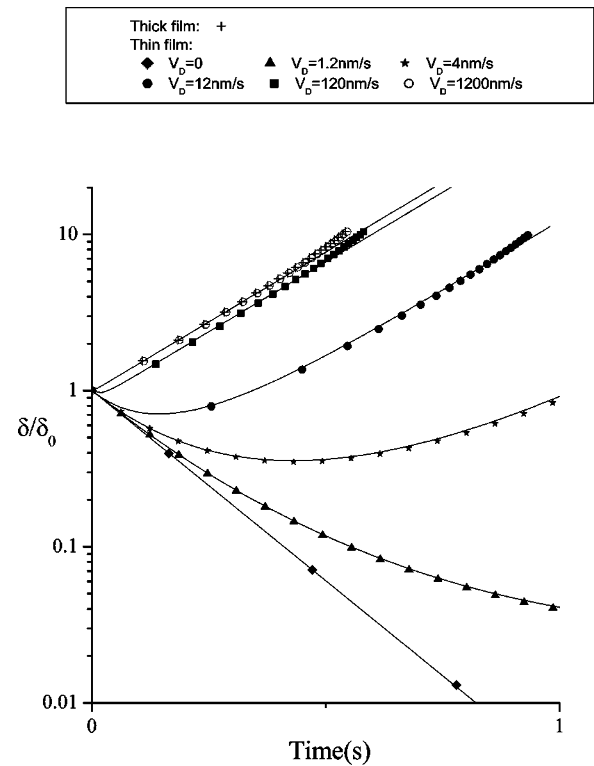

FIG. 10. Film growth when surface tension is isotropic and deposition is constant in the y direction. The symbols represent the numerical simulation results and the lines the linear evolution equation values. $k = 0.75\times 2M\varepsilon^2/\tilde{\gamma}_0$. The parameters used are the same as those in Fig. 9.

by linear analysis. However this growth slows and the graph approaches the flat line representative of a steady-state morphology. Note that in comparison when deposition is constant in the vertical y direction (shown as circles in Fig. 9), the film evolves according to the linear evolution equation. Under deposition perpendicular to the film surface, when a cusp begins to form, material is deposited more rapidly on the steep cusp slope, hence slowing cusp formation. When deposition is constant vertically it only effects surface evolution indirectly by raising the average surface height. Though deposition rates of this magnitude are not generally used in experiment it is nevertheless physically interesting to observe the difference in surface evolution between the two growth methods.

When the deposition is constant in the vertical y direction, the film evolves according to the linear evolution equation, even after the surface is no longer a sine function and cusp formation occurs. This can be seen in Fig. 10 which compares results from the numerical simulation with the results predicted by the linear evolution Eq. (26). Figure 8 shows a very clear cusp formation in the surface morphology, while for the same time Fig. 10 shows the sharp cusp growing only slightly faster than predicted by linear analysis. This slight deviation is expected as the stress in a cusp valley is larger than in a sine valley hence accelerating perturbation growth.

When the surface tension is anisotropic the surface evolution is very different from that predicted by the linear analysis. As can be seen in Fig. 10, a perturbation in an isotropic film decays until the film surface reaches a height at which the film is linearly unstable to perturbations at that wavelength. No matter how large the deposition rate, at any given time a perturbation in a thin film is always smaller than a perturbation of the same initial size in an infinite film due to the finite time spent in the linear wetting layer.

When surface tension is anisotropic, initially the perturbation amplitude decreases as the surface facets. The rate and amplitude of the decrease are independent of either C or V_D. The film then grows or decays depending on whether the perturbation amplitude $\delta(t)$ is larger or smaller than the critical perturbation amplitude $\delta_c(k,h)$, at $h = V_D t + C$. When $\delta_0 > \delta_c(k,h=C)$ the perturbation grows immediately after faceting. When $\delta_0 < \delta_c(k,h=C)$ the perturbation initially decays though it will start to grow again if the deposition brings the film surface to a height at which $\delta(t) > \delta_c(k,h = V_D t + C)$.

We now turn to characterize the evolution of the film in terms of all the relevant physical variables. There are five independent variables that can effect the evolution: V_D, C, k, t, and ε. In addition, there are four relevant constant parameters: h_{ml}, K, $\tilde{\gamma}_0$, and M. We can replace the five independent variables by the dimensionless variables $V_D t/h_{ml}$, C/h_{ml}, $K\tilde{\gamma}_0 k^4 t$, $KM\varepsilon^2 k^3 t$, and $KM\varepsilon^2 k^2 t/h_{ml}$. The idea is

that the description of the evolution of a film with isotropic surface tension becomes simpler in terms of these variables. This becomes clear when we look at how a perturbation in a thin film grows in relation to the growth of a perturbation of the same initial size in an infinite film. Quantitatively, this is described by the relative perturbation height, $\delta_R = \delta(t,C)/\delta(t,C=\infty)$. As can be seen from Eq. (26), δ_R depends only on three of the five independent dimensionless variables:

$$\delta_R = \left[\exp K k^2 \chi \frac{M\varepsilon^2}{2V_D} \right] \exp(-C/h_{ml})[\exp(-V_D t/h_{ml}) - 1]. \quad (27)$$

This can be summarized in the scaling law

$$\delta_R(V_D, C, k, t, \varepsilon) = \delta_R(V_D t/h_{ml}, C/h_{ml}, KM\varepsilon^2 k^2 t/h_{ml}), \quad (28)$$

which implies that δ_R depends only on three of the five scaling variables. The manifestation of this scaling behavior is data collapse. For example, when $V_D=0$ and C is fixed, all the curves of $\delta_R(t)$ for different values of k and ε fall onto a single curve if plotted as a function of $k^2\varepsilon^2 t$ rather than t.

Does this scaling law survive beyond linear analysis? We looked for scaling when deposition was constant in the vertical y direction for both isotropic and anisotropic surface tension. As mentioned earlier when surface tension is isotropic the film continued to evolve according to the linear evolution Eq. (26) long after it left the linear regime and hence the scaling relation (28) also held.

Growth under anisotropic surface tension is very different from that given by the linear evolution Eq. (26), and hence the scaling relation (28) does not hold. Does this mean that the physics of anisotropic surfaces is more complicated and depends on all five independent variables? It turns out the answer to this question is "*no*" to a good approximation. To see this we define five generalized dimensionless variables: $V_D t/h_{ml}$, C/h_{ml}, $K\tilde{\gamma}_0 k^4 t$, $KM\varepsilon^2 k^3 t$, and $K\tilde{\gamma}_0^{p+q/2+1} M^{-p-q/2} \varepsilon^{-2p-q} k^p t/h_{ml}^{q/2+4}$. When $p=2$ and $q=-6$ we regain the dimensionless variables governing the linear evolution equation. We found numerically that in the case of anisotropic surface tension, δ_R approximately obeys the scaling law:

$$\delta_R(k, V_D, \varepsilon, t, C) = \delta_R(V_D t/h_{ml}, C/h_{ml}, K\tilde{\gamma}_0^{p+q/2+1} M^{-p-q/2} \times \varepsilon^{-2p-q} k^p t/h_{ml}^{q/2+4}) \quad (29)$$

with $p \sim 2.37$ and $q \sim -6.5$. Again, δ_R depends only on three of the five scaling variables, which implies data collapse. This relation was very robust. We verified it for different G, variation of k of an order of magnitude, variation of ε by 100%, and deposition rates of between 0 and 120 000 Å/s. Figures 11 and 12 show this scaling in the form of data collapse when $C=2$ ML. Data collapse when δ_R is plotted against a variable proportional to the third scaling variable in Eq. (29) can be seen in Fig. 11. Here there is no deposition, k varies by over an order of magnitude, and ε by 100%. As can be seen the data collapse is not exact but holds to a good approximation. Figure 12 shows data collapse when δ_R is plotted against variables proportional to the first and third scaling variables in Eq. (29). Deposition rates vary by six orders of magnitude, k varies by over an order of magnitude, and ε by 100%. Data collapse is shown by all curves falling onto a single surface.

The scaling relationship (29), however, only held when the initial perturbation δ_0 was larger than the critical perturbation at that wave number, k, and initial film height, C, i.e.,

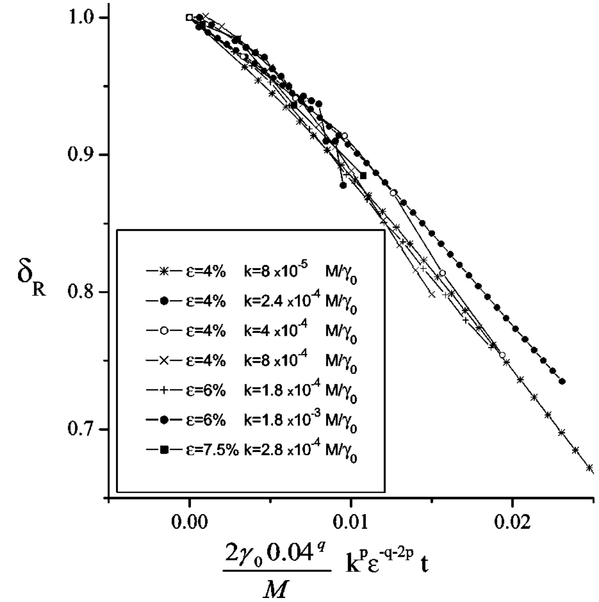

FIG. 11. Scaling of relative perturbation height for different k ($k=8\times10^{-5}M/\gamma_0 \rightarrow 2\times10^{-3}M/\gamma_0$) and ε ($\varepsilon=4\% \rightarrow 7.5\%$) with zero deposition. $p=2.37$ and $q=-6.5$. Note that the variable used to plot this graph $(2\gamma_0 0.04^q/M)k^p\varepsilon^{-2p-q}t$ is proportional to the scaling variable $K\tilde{\gamma}_0^{p+q/2+1}M^{-p-q/2}\varepsilon^{-2p-q}k^p t/h_{ml}^{q/2+4}$.

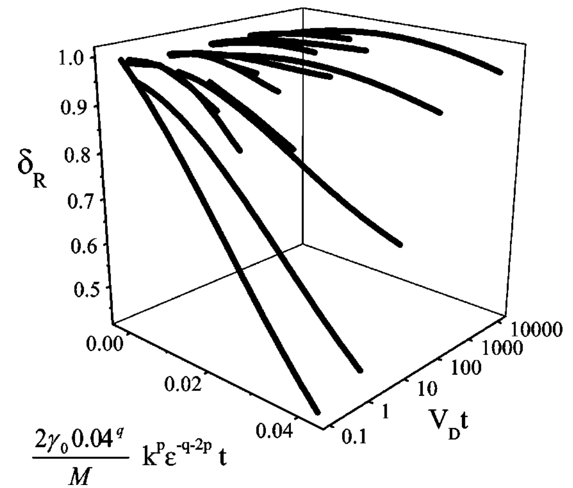

FIG. 12. Scaling of relative perturbation height for different k ($k=8\times10^{-5}M/\gamma_0 \rightarrow 2\times10^{-3}M/\gamma_0$), ε ($\varepsilon=4\% \rightarrow 7.5\%$), and V_D ($V_D=0,0.12,1.2,12,120,1200,12\,000,120\,000$ Å/s). $p=2.37$ and $q=-6.5$. Note that the variables used to plot this graph $(2\gamma_0 0.04^q/M)k^p\varepsilon^{-2p-q}t$ and $V_D t$ are proportional to the scaling variables $K\tilde{\gamma}_0^{p+q/2+1}M^{-p-q/2}\varepsilon^{-2p-q}k^p t/h_{ml}^{q/2+4}$ and $V_D t/h_{ml}$.

for $\delta_0 > \delta_c(k,C)$. This is probably because when $\delta_0 > \delta_c(k,C)$ perturbations of a thin film and of an infinite film evolve similarly. Both perturbations initially decay while faceting and then continue to grow. On the other hand, when $\delta_c(k,\infty) < \delta_0 < \delta_c(k,C)$ a perturbation of a thin film decays whereas an infinite-film perturbation facets and grows. In this regime scaling laws were not found. When $\delta_0 < \delta_c(k,\infty)$ the perturbation decays in both the thin and infinite films. When δ_0 is small enough the scaling laws (28) derived from the linear evolution equation are regained.

ACKNOWLEDGMENTS

We would like to thank J. Tersoff, B.J. Spencer, and V.I. Marchenko for interesting discussions relating to matter contained in this paper.

*Electronic address: hrg1000@wicc.weizmann.ac.il
†Electronic address: daniel.kandel@weizmann.ac.il http://www.weizmann.ac.il/~fekandel

[1] D.J. Eaglesham and M. Cerullo, Phys. Rev. Lett. **64**, 1943 (1990).
[2] Y.-W. Mo, D.E. Savage, B.S. Swartzentruber, and M.G. Lagally, Phys. Rev. Lett. **65**, 1020 (1990).
[3] J. Massies and N. Grandjean, Phys. Rev. Lett. **71**, 1411 (1993).
[4] T.R. Ramachandran, R. Heitz, P. Chen, and A. Madhukar, Appl. Phys. Lett. **70**, 640 (1997).
[5] T.I. Kamins, E.C. Carr, R.S. Williams, and S.J. Rosner, J. Appl. Phys. **81**, 211 (1997).
[6] J.A. Floro, E. Chason, R.D. Twesten, R.Q. Hwang, and L.B. Freud, Phys. Rev. Lett. **79**, 3946 (1997).
[7] J.A. Floro, E. Chason, L.B. Freund, R.D. Twesten, R.Q. Hwang, and G.A. Lucadamo, Phys. Rev. B **59**, 1990 (1999).
[8] R.M. Tromp, F.M. Ross, and M.C. Reuter, Phys. Rev. Lett. **84**, 4641 (2000).
[9] D.D. Perovic, B. Bahierathan, H. Lafontaine, D.C. Houghton, and D.W. McComb, Physica A **239**, 11 (1997).
[10] H.J. Osten, H.P. Zeindl, and E. Bugiel, J. Cryst. Growth **143**, 194 (1994).
[11] C.-H. Chiu and H. Gao, Mater. Res. Soc. Symp. Proc. **356**, 33 (1995).
[12] B.J. Spencer, Phys. Rev. B **59**, 2011 (1999).
[13] J. Tersoff, Phys. Rev. B **43**, 9377 (1991).
[14] I. Daruka and A.-L. Barabási, Phys. Rev. Lett. **79**, 3708 (1997).
[15] L.G. Wang, P. Kratzer, M. Scheffler, and N. Moll, Phys. Rev. Lett. **82**, 4042 (1999); L.G. Wang, P. Kratzer, N. Moll, and M. Scheffler, Phys. Rev. B **62**, 1897 (2000).
[16] C. Roland and G.H. Gilmer, Phys. Rev. B **47**, 16 286 (1993).
[17] A.J. Pidduck, D.J. Robbins, A.G. Gullis, W.y. Leong, and A.M. Pitt, Thin Solid Films **222**, 78 (1992); W. Dorsch, B. Steiner, M. Albrecht, H.P. Strunk, H. Wawra, and G. Wagner, J. Cryst. Growth **183**, 305 (1998); K.M. Chen, D.E. Jesson, S.J. Pennycook, T. Thundat, and R.J. Warmack, Phys. Rev. B **56**, R1700 (1997).
[18] H.R. Eisenberg and D. Kandel, Phys. Rev. Lett. **85**, 1286 (2000).
[19] W.W. Mullins, J. Appl. Phys. **28**, 333 (1957).
[20] I.S. Sokolnikoff, *Mathematical Theory of Elasticity* (McGraw-Hill, New York, 1946).
[21] V.I. Marchenko and A.Ya. Parshin, Zh. Éksp. Teor. Fiz. **79**, 257 (1980) [Sov. Phys. JETP **52**, 129 (1980)].
[22] S. Timoshenko and J.N. Goodier, *Theory of Elasticity* (McGraw-Hill, New York, 1951).
[23] S.G. Mikhlin, *Integral Equations* (Pergamon, New York, 1957).
[24] H.P. Bonzel and E. Preuss, Surf. Sci. **336**, 209 (1995).
[25] R.J. Asaro and W.A. Tiller, Metall. Trans. **3**, 1789 (1972); D.J. Srolovitz, Acta Metall. **37**, 621 (1989); M.A. Grinfeld, Dokl. Akad. Nauk (SSSR) 290, 1358 (1986) [Sov. Phys. Dokl. **31**, 831 (1986)].
[26] C. Herring, Phys. Rev. **82**, 87 (1951).
[27] R.V. Kukta and L.B. Freund, J. Mech. Phys. Solids **45**, 1835 (1997).
[28] R.P. Feynman, R.B. Leighton, and M. Sands, *The Feynman Lectures on Physics* (Addison-Wesley, Reading, MA, 1965), Vol. II, Chap. 39, Sect. 5.
[29] B.J. Spencer and D.I. Meiron, Acta Metall. Mater. **42**, 3629 (1994).
[30] F. Long, S.P.A. Gill, and A.C.F. Cocks, Phys. Rev. B **64**, 121307 (2001).